View metadata, citation and similar papers at core.ac.uk
brought to you by CORE
provided by Universiti Teknikal Malaysia Melaka (UTeM) Repository

BRAIN LESION SEGMENTATION FROM DIFFUSION-WEIGHTED MRI BASED ON ADAPTIVE THRESHOLDING AND GRAY LEVEL CO-OCCURRENCE MATRIX

Norhashimah Mohd Saad[1], S.A.R. Abu-Bakar[2], Abdul Rahim Abdullah[3], Lizawati Salahuddin[1], Sobri Muda[4], Musa Mokji[2]

[1]Faculty of Electronics & Computer Engineering, Universiti Teknikal Malaysia Melaka, Malaysia

[2]Faculty of Electrical Engineering, Universiti Teknologi Malaysia, Malaysia

[3]Faculty of Electrical Engineering, Universiti Teknikal Malaysia Melaka, Malaysia

[4]Radiology Department, Medical Centre, Universiti Kebangsaan Malaysia, Malaysia

Email: [1]norhashimah@utem.edu.my, [2]syed@fke.utm.my, [3]abdulr@utem.edu.my, [1]lizawati@utem.edu.my, [4]sobri_muda@yahoo.com, [3]musa@fke.utm.my

Abstract

This project presents brain lesion segmentation of diffusion-weighted magnetic resonance images (DWI) based on thresholding technique and gray level co-occurrence matrix (GLCM). The lesions are hyperintense lesion from tumour, acute infarction, haemorrhage and abscess, and hypointense lesion from chronic infarction and haemorrhage. Pre-processing is applied to the DWI for intensity normalization, background removal and intensity enhancement. Then, the lesions are segmented by using two different methods which are thresholding technique and GLCM. For the thresholding technique, image histogram is calculated at each region to find the maximum number of pixels for each intensity level. The optimal threshold is determined by comparing normal and lesion regions. Conversely, GLCM is computed to segment the lesions. Different peaks from the GLCM cross-section indicate the present of normal brain region, cerebral spinal fluid (CSF), hyperintense or hypointense lesions. Minimum and maximum threshold values are computed from the GLCM cross-section. Region and boundary information from the GLCM are introduced as the statistical features for segmentation of hyperintense and hypointense lesions. The proposed technique has been validated by using area overlap (AO), false positive rate (FPR), false negative rate (FNR), misclassified area (MA), mean absolute percentage error (MAPE) and pixels absolute error ratio (r_{err}). The results are demonstrated in three indexes MA, MAPE and r_{err}, where 0.3167, 0.1440 and 0.0205 for GLCM, while 0.3211, 0.1524 and 0.0377 for thresholding technique. Overall, GLCM provides better segmentation performance compared to thresholding technique.

Keywords: *DWI, GLCM, segmentation, thresholding.*

I. INTRODUCTION

Tumor, infarction (stroke/ischemia), haemorrhage (bleeding/ ischemia) and infection (abscess) are the example of brain lesions that are affected in the brain cerebrum. In 2006, it was reported that tumor and brain diseases such as brain infarction and haemorrhage were the third and fourth leading cause of death in Malaysia [1]. The incidence of brain tumor in 2006 was 3.9 among males and 3.2 among females per 100,000 populations with a total of 664 cases reported by the

This work was supported by Universiti Teknikal Malaysia Melaka (UTeM) under Short Term Grant PJP/2010/FKEKK (30D) S770.

Minister of Health Malaysia. In the United States, the combined incidence of primary brain tumor was 6.6 per 100,000 persons per year with a total of 22,070 new cases in 2009 [2], while brain infarction affects approximately 750,000 new cases per year [3].

Interpretation of brain imaging plays an important part in diagnosis of various diseases and injury. Magnetic resonance imaging (MRI) is one of the popular, painless, non-radiation and non-invasive brain imaging techniques. Nevertheless, assessment of brain lesion in MRI is a complicated process and typically performed by experienced neuroradiologists. An expert neuroradiologist performs this task with a significant degree of precision and accuracy. It can often be difficult for clinicians to precisely assess the lesion on the basis of radiographic appearance. Therefore, quantitative analysis using computers can help radiologists to overcome these problems. Due to the importance of brain imaging interpretation, significance research efforts have been devoted for developing better and more efficient techniques in several related areas including processing, modeling and understanding of brain images [4].

Over the past several years, developments in MRI unit have enabled the acquisition of MR imaging using fast and advanced techniques, proving extremely useful in various clinical and research applications such as diffusion-weighted MRI (DW-MRI or DWI) [5]. DWI proficient to provide image contrast that is dependent on the molecular motion of water, which can alter by disease [6]. The image is bright (hyperintense) when the rate of water diffusion in the cell membrane is restricted and dark (hypointense) when the diffusion is elevated [6]. DWI provides very good lesion contrast compared to the appearance in conventional MRI [3]. Research have shown DWI is considered as the most sensitive technique in detecting early acute neurological disorders, stroke, infection, trauma and tumor [3,6-7].

Segmentation or separation of specific region of interest (ROI) of pathological abnormalities from MR images is an essential process for diagnosis and treatment planning. Accurate segmentation is still a challenging task because of the variety of the possible shapes, locations and image intensities of various types of problems and protocols. Computerized segmentation process is essential to overcome these problems. A large number of approaches have been proposed by various researchers to deal with various MRI protocols [8]. These approaches were introduced to solve the problems of automatic lesion detection and segmentation in various conventional MRI.

Thresholding based segmentation discriminates pixels according to their gray level value. The key parameter in the thresholding process is the choice of the threshold value. In this study, histogram thresholding is applied to separate hyperintense lesion from DW images. The rationale being that the brightness of hyperintense lesion pixels are higher than the normal pixels.

Gray level co-occurrence matrix (GLCM) has been widely used in computer vision and pattern recognition applications [9] such as in fingerprint verification [10], fruits skin defect detection [11], industrial vision system [12], and in medical image analysis (notably on x-ray, MRI, echocardiogram and mammogram) in order to discriminate between pathological and non-pathological tissues [13-16]. In the classical technique, Haralick et al. [17] introduced six textural features from GLCM which are the most relevant features to analyze textural images. This method has been widely used by various researchers for segmenting or identifying tissue types in MR images [18, 14, 19-24]. In this research work, a new approach for automatically detecting and segmenting brain lesions from DWI is introduced.

Beside the widely known thresholding, this paper proposes a new statistical information based on region and boundary information from the GLCM. The analysis involves both thresholding and GLCM computation to pre-processed DWI; calculating the minimum and maximum threshold values from GLCM cross-section; and segmenting the hyperintense or hypointense lesions based on thresholding and region and boundary information from the GLCM. Segmentation evaluation is made in order to analyze the performance of the proposed techniques.

II. DIFFUSION-WEIGHTED MRI

A. Brain Lesion

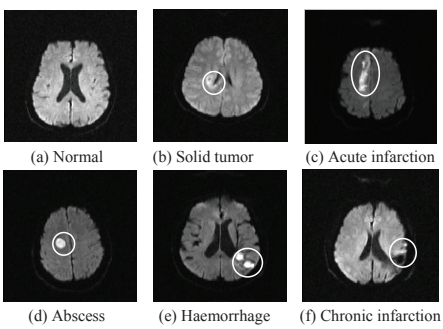

(a) Normal (b) Solid tumor (c) Acute infarction

(d) Abscess (e) Haemorrhage (f) Chronic infarction

Fig. 1 Original DWI with brain lesion indicated by a white circle

Fig. 1 shows DWI intensities in major brain lesion, where the lesion is indicated by a white circle. In normal brain, the region consists of brain tissue (normally called as gray and white matter tissue in conventional MRI) and a cavity which is full of cerebral spinal fluid (CSF) located in the middle of the brain, as shown in Fig. 1(a). The DWI intensity for CSF is dark. Fig. 1 (b-f) shows several brain lesions, in which the intensity can be divided into hyperintense and hypointense.

DWI hyperintense lesion includes acute infarction, acute haemorrhage, solid tumor and abscess. Chronic infarction and necrosis tumor appear to be hypointense in DWI. The summary of major brain lesions, types, symptoms and pathological findings is summarized in Table I. Nevertheless, this paper is only focused on the hyperintense lesions. Based on our hypothesis, the hyperintense lesions in DWI can be well separated from the normal tissue because of its high gray level intensity.

Table 1 Description of brain lesions, types, symptoms and pathological findings [25-28]

Brain Lesion	DWI Characteristics	Symptoms	Pathological Findings
Tumor	**Solid:** Hyperintense **Cystic/ Necrosis:** Hypointense	Loss of balance; walking, visual and hearing problems; headache; nausea; vomiting; unusual sleep; seizure	Abnormal growth of cells in uncontrolled manner **shape:** round, ellipse, irregular **texture:** clear, partially clear, blur
Infarction (Stroke/ Ischemia)	**Acute** (30 minutes - 72 hours after onset): Hyperintense **Chronic** (after 2 weeks): Hypointense	Paralysis; visual disturbances; speech problems; gait difficulties; altered level of consciousness	Cerebral vascular occlusion/ blockage
Haemorrhage (Bleeding/ Ischemia)	**Deoxyhemoglo -bin:** Hyperintense **Oxyhemoglo-bin:** Hypointense	Paralysis; unconsciousness; visual disturbances; speech problems	Presence of blood products outside of the cerebral vascular
Infection (Abscess)	Hyperintense	Fever; seizure; headache; nausea; vomiting; altered mental status	Bacterial, viral or fungal infections, inflammatory and pus

B. Imaging Parameter

The DW images have been acquired from the General Hospital of Kuala Lumpur using 1.5T MRI scanners Siemens Magnetom Avanto. Acquisition parameters used were time echo (TE), 94 ms; time repetition (TR), 3200 ms; pixel resolutions, 256 x 256; slice thickness, 5 mm; gap between each slice, 6.5 mm; intensity of diffusion weighting known as b value, 1000 s/mm^2 and total number of slices, 19. All samples have medical records which have been confirmed by neuroradiologists. Images were encoded in 12-bit DICOM (Digital Imaging and Communications in Medicine) format.

III. PROPOSED TECHNIQUES

A. Thresholding Technique

The flowchart of the proposed segmentation is shown in Fig. 2. The samples of brain DWI dataset are first collected. In the pre-processing stage, several algorithms are applied to enhance the images. The intensity is normalized from 0 to 1, the background and skull are removed and then the intensity is enhanced using two different algorithms which are gamma-law transformation and contrast stretching. The algorithms are applied to span the narrow range of DWI histogram for thresholding purpose. The segmentation process starts at full image and splits to 8 x 8 regions. The lesion intensity range is analysed based on thresholding technique. This is done by calculating image histogram at each region and finding the maximum number of pixels at each intensity level. An optimal threshold is determined by comparing normal and lesion regions in the histogram. Region of interest (ROI) is then segmented based on the optimal threshold.

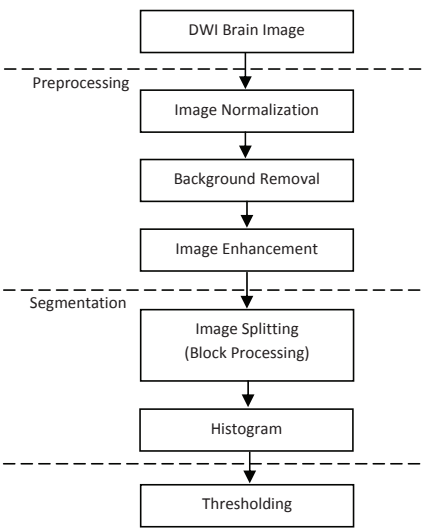

Fig. 2 Flowchart of the proposed thresholding technique

B. GLCM

GLCM [17, 29] is a matrix of relative frequencies in which two neighbouring pixels separated by distance *d*, at angular orientation ϕ, occur in an image. One pixel is with gray level u and the other is with gray level *v*. The angular orientation ϕ is quantized to four directions which are horizontal, diagonal, vertical and off-diagonal, or 0^o, 45^o, 90o and 135^o, respectively. For an image I(x,y), where the image has $1 \le x \le N_x$ pixels in horizontal direction and $1 \le y \le N_y$ pixels in vertical direction. Suppose that the image has Ng resolution levels in which u represents the gray level of pixel I(x,y) and v represents the gray level of the nearest-neighbour pixel where $0 \le u,v \le N_g-1$. The GLCM, $G(u,v)_{d,\phi}$ is calculated as:

$$G(u,v)_{d,\phi} = \sum_{x=1}^{N_x}\sum_{y=1}^{N_y} \begin{cases} 1 & \text{if } u = I(x,y) \text{ and } v = v_{d,\phi} \\ 0 & \text{otherwise} \end{cases} \quad (1)$$

$v_{d,\phi}$ is referred to the nearest neighbour pixel, defined as:

$$v_{d,\phi} = \begin{cases} I(x, y \pm d) & \text{for } \varphi = 0^o \\ I(x \mp d, y \pm d) & \varphi = 45^o \\ I(x \mp d, y) & \varphi = 90^o \\ I(x \mp d, y \mp d) & \varphi = 135^o \end{cases} \quad (2)$$

For *d*=1, the eight nearest-neighbour orientation of ϕ corresponding to pixel I(x,y) can be illustrated in Fig. 3.

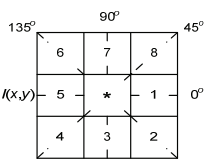

Fig. 3 Eight nearest-neighbour pixel cells to pixel *. With d=1; 1 and 5 areϕ = 0^o, 4 and 8 are ϕ = 45^o, 3 and 7 are ϕ = 90^o, 2 and 6 are ϕ = 135^o. * is the reference pixel I(x,y) [17].

One of the characteristic of the GLCM is it is diagonally symmetry. Thus, the corresponding adjacent pixel $v_{d,\phi}$ such in equation (2) can be simplified as:

$$v_{d,\phi} = \begin{cases} I(x, y+d) & \text{for } \varphi = 0^o \\ I(x-d, y+d) & \varphi = 45^o \\ I(x-d, y) & \varphi = 90^o \\ I(x-d, y-d) & \varphi = 135^o \end{cases} \quad (3)$$

In practice, for each *d*, the matrices for the four orientations are averaged. Thus, the averaged GLCM, $G(u,v)$ is computed as:

$$G(u,v) = \frac{1}{4}\left(G(u,v)_{d,0^o} + G(u,v)_{d,45^o} + G(u,v)_{d,90^o} + G(u,v)_{d,135^o}\right) \quad (4)$$

IV. IMAGE PREPROCESSING

Several Several pre-processing algorithms are applied to DW images for intensity normalization, background removal and intensity enhancement. The original DWI has 12-bit intensity depth unsigned integer. In normalization process, the type of the intensity depth is converted to double precision, where the minimum value is set to 0 while for the maximum is to 1. The DWI includes background image which needs to be removed. This is because the background shares similar gray level values with certain brain structures. The technique for background removal can be found in [30]. Then, image enhancements are applied. Two different techniques are used, which are Gamma-law transformation algorithm and contrast stretching. The objective is to evaluate image enhancement that can provide better segmentation results for thresholding technique.

Gamma-law transformation algorithm is chosen to expand the narrow range of low input gray level values of DWI to a wider range. It has the basic form of $s=cr^{\gamma}$, where *c* is amplitude, and γ is a constant power of input gray level, r [31]. γ=0.4 has been found to be the best value based on experiments to enhance the output histogram [32]. The Gamma-law transformation response is shown in Fig. 4.

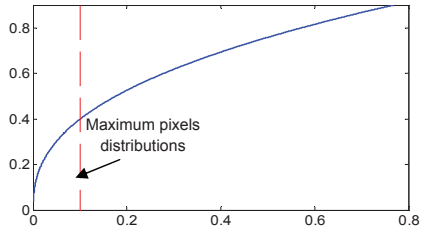

Fig. 4 Image response for gamma-law transformation

On the other hand, contrast stretching is applied to improve an image by stretching the range of intensity values. Unlike histogram equalization, contrast stretching is restricted to a linear mapping of input to output values. For each pixel, the input gray level, *r* is mapped to output, *s* according to equation (5).

$$s = ratio * r \quad (5)$$

where ratio is:

$$ratio = \frac{\text{Original Image Background}}{\text{Standardize Image Background}} \quad (6)$$

Standardize Image Background = 0.02 is adopted for this experiment. This value is chosen to correct the image background in-homogeneity. Thus, the images will have similar background value, with the average of 0.02.

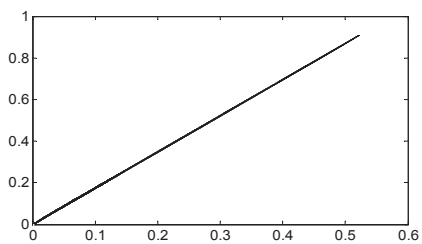

Fig. 5 Image response for contrast stretching

Fig. 5 shows image response of contrast stretching in which the original value, r is mapped to output value, s. Fig. 6 illustrates the results of preprocessing steps. Fig. 6(a) shows the original normalized image and its histogram. In Fig. 6(b), all background pixels have been removed, and therefore improve the shape of the

image histogram. The maximum peak is located at 0.1. After applying Gamma-law transformation algorithm, the histogram has been enhanced in which the peak is located at 0.4 as shown in Fig. 6(c). On the other hand, the maximum peak is located at 0.2 for contrast stretching as shown Fig. 6(d).

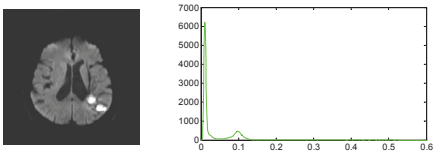

(a) Image and histogram of intensity normalization

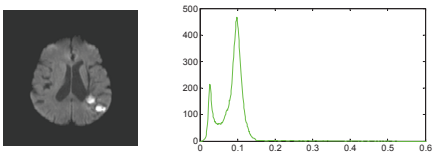

(b) Image and histogram of background removal

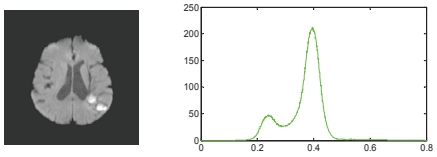

(c) Image and histogram of Gamma-law transformation

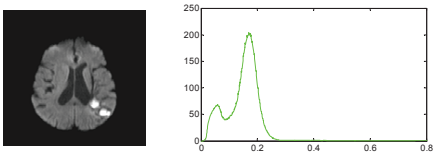

(d) Image and histogram of contrast stretching

Fig. 6 Pre-processing steps

V. SEGMENTATION PROCESS USING THRESHOLDING TECHNIQUE

For the image segmentation process, firstly the entire image is divided by 8 x 8 regions where 256 x 256 pixels of the entire image is split to 16 x 16 pixels size in each region. Fig. 7 shows the image splitting (block processing) with 16 x 16 pixels size per segment.

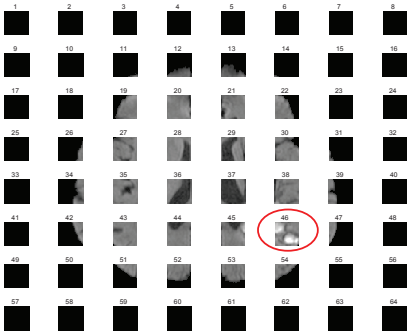

Fig. 7 Image splitting (16 x 16 pixels size per segment)

Region 46 which is indicated by red circle is the lesion, examine by neuroradiologist. Next, histogram is calculated at each region as shown in Fig. 8. The red circle shows the histogram distribution of lesion, whereas the others are histogram of normal brain area.

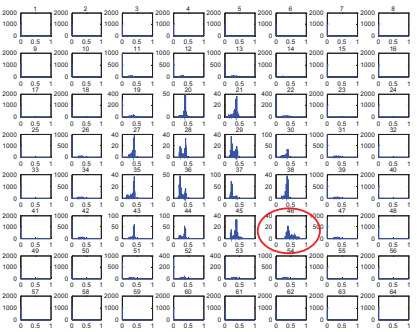

Fig. 8 Histogram distribution of each region

Two histograms which are normal and abnormal (lesion) are then generated. All normal and abnormal regions are overlap respectively to find the maximum number of pixels at each intensity level. The maximum number of pixels is calculated by using the function shown in equation (7).

$$\text{Max Pixels}(n) = \text{Max}(\text{Pixels}\ (R_1 : R_m, n)) \qquad (7)$$

Where n is the intensity at level n, R1 and Rm are regions in the block histogram according to each intensity level. The purpose of overlapping the histogram

for each block is to enhance the lesion for comparison with normal. This will produce a new histogram as shown in Fig. 9. The optimal threshold is determined by the ROI indicator, which the intensity level of normal histogram is reached zero pixels.

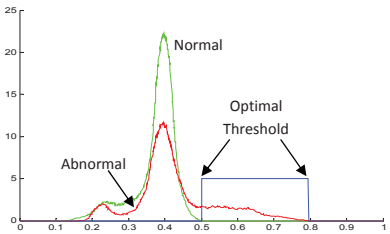

Fig 9 Optimal threshold with Gamma-law enhancement

Fig. 10 shows the maximum block histogram, which is done by overlapping the histogram in all blocks including both normal and abnormal. By using the proposed technique, we can clearly characterize the lesion area because it has been enhanced.

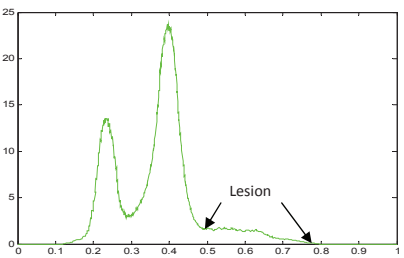

Fig 10 Maximum block histogram

The statistical features representing the hyperintense and hypointense regions are then calculated according to equation (8), where $T_{optimal}$ is the threshold value to obtain the segmentation.

$$I(x,y)_{hyperintense} = \begin{cases} 1 \text{ for } I(x,y) \geq T_{optimal} \\ 0 \text{ elsewhere} \end{cases} \quad (8)$$

VI. SEGMENTATION PROCESS USING GLCM

Fig. 11 shows an example of GLCM for image in Fig. 1(c). The image has hyperintense lesion due to acute infarction. The GLCM is computed for Ng=128, d=1 and at average orientations, and is represented in a contour plot. Colour intensity represents the co-occurrence frequencies, or the number of repetitions between each pixel pair, u and v. It can be seen that hypointense region and CSF occur at smaller co-occurrence entry; normal brain tissue is located in the middle of the matrix, while hyperintense region exists at higher entry. The red dash-line shows a cross-section at u=v. At this line, the co-occurrence frequency is the highest. The plot also shows that the co-occurrence frequencies are diagonally symmetry and the gray level resolutions are brighter when the co-occurrence transitions increase off-diagonally with the matrix.

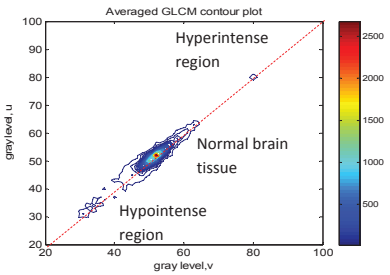

Fig. 11 GLCM for DWI in Fig. 1(c)

A. Minimum and Maximum Threshold

The GLCM G(u,v) is basically shows a representation of a second-order histogram in which the (u,v)th element is the frequency that pixel pair *u* co-occurs with *v*. GLCM cross-section can be constructed in which each entry at *u=v* is plotted versus the frequency. Fig. 12 shows the GLCM cross-section from the contour plot in Fig. 11.

The maximum peak of the cross-section shows the normal brain region. The CSF and the hyperintense lesion are indicated

by very small peaks at the smaller and higher entry, respectively. The magnitudes of the peaks depend on the size of lesions. To find the minimum and maximum threshold values, the gradient function, or the divergence slope is calculated. The gradient reach maximum when the GLCM frequency is the greatest rate of change, and vice versa. The minimum and maximum threshold (T_1 and T_2) is set at the first zero-gradient before and after the maximum peak, respectively.

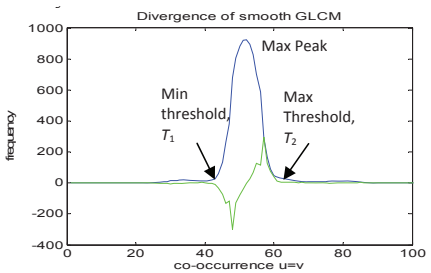

Fig. 12 GLCM Cross-section and the divergence slope to determine the minimum and maximum threshold values

B. Region and Boundary Information from GLCM

In this research, the region and boundary information are based on the partition of nine regions, which are separated by the minimum and maximum threshold values, T_1 and T_2. Referring to Fig. 13, region 1 represents hypointense; region 2 represents normal brain tissue while region 3 represents hyperintense. The boundary between each region is then represented in region 1, 2; 1, 3 and 2, 3. Each boundary has two regions due to the symmetrical feature of the GLCM.

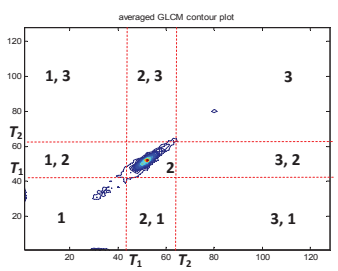

Fig. 13 Gray level region and boundary information

C. Segmentation

The statistical features representing the hyperintense and hypointense regions are then calculated according to equation (9) and (10) as follow:

$$G(u,v)_3 = \begin{cases} G(u,v) & \text{for } u \geq T_2 \text{ and } v \geq T_2 \\ 0 & \text{elsewhere} \end{cases} \quad (9)$$

$$G(u,v)_1 = \begin{cases} G(u,v) & \text{for } u \leq T_1 \text{ and } v \leq T_1 \\ 0 & \text{elsewhere} \end{cases} \quad (10)$$

where $G(u,v)_3$ and $G(u,v)_1$ is the region for hyperintense and hypointense, respectively. Segmentation image for hyperintense and hypointense lesions are then computed. For hyperintense, its segmentation image $I_3(x,y)$ is computed for $1 \leq x \leq N_x$; $1 \leq y \leq N_y$ and $0 \leq u,v \leq N_g$-1, as below:

$$I_3(x,y) = \sum_{x=1}^{N_x} \sum_{y=1}^{N_y} \begin{cases} 1 & \text{if } G(u,v)_3 > 0 \\ 0 & \text{elsewhere} \end{cases} \quad (11)$$

$G(u,v)_3$ is the sum of angular orientations, such that

$$G(u,v)_3 = G(u,v)_{3,d,0^o} + G(u,v)_{3,d,45^o} + G(u,v)_{3,d,90^o} + G(u,v)_{3,d,135^o} \quad (12)$$

where $u=I(x,y)$ and v is the nearest-neighbour pixels as in equation (3). Similar computation can be done for the hypointense lesion. In general, the example of the segmentation for d=1 and $\phi=0^o$ is as follow:

loop x, y
  $u = I(x,y)$;
  $v = I(x, y+1)$;
  if $G(u,v)_{segm} > 0$
    $I_{segm}(x,y) = 1$;
  end
end loop

VII. PERFORMANCE ASSESSMENT METRICS

Performance assessment of the segmentation results is done by comparing the ROI obtained from the automatic segmentation with the reference ROI provided by neuroradiologists. Area overlap (AO) also known as Jaccard statistical index, false positive rate (FPR), false negative rate (FNR) and misclassified area (MA) are used as the performance metrics. These metrics are computed as follows [33]:

$$AO = \frac{S_1 \cap S_2}{S_1 \cup S_2} \tag{13}$$

$$FPR = \frac{S_1 \cap S_2^c}{S_1 \cup S_2} \tag{14}$$

$$FNR = \frac{S_1^c \cap S_2}{S_1 \cup S_2} \tag{15}$$

$$MA = 1 - AO = FPR + FNR \tag{16}$$

where S_1 represents the segmentation results obtained by the segmentation algorithms and S_2 represents the manual segmentation provided by the neuroradiologists. c is the complement of S_1 and S_2. AO computes the segmented similarity by comparing the overlap region between the manual and the automatic segmentation. FPR and FNR are used to quantify oversegmentation and undersegmentation respectively. High AO, low FPR, FNR and MA show low error, i.e. high accuracy of the measurement.

Mean absolute percentage error (MAPE) was used as index for misclassified index for mean and number of pixels value in the segmentation area, while pixel absolute error ratio (rerr) was for misclassified pixels for normal control. MAPE is an index that measures the difference between actual and measured value and is expressed as:

$$MAPE = 100 \times \frac{|S_1 - S_2|}{S_1} \tag{17}$$

Besides MAPE, absolute error ratio, r_{err} was also applied to quantify the accuracy of the segmentation for normal image. rerr is defined as the ratio between the absolute difference in the number of over segmented pixels between the actual and the proposed segmentation method, n_{diff}, and the total number of pixels, N, of an image. Normal image should result 0 number of pixel in the segmented image. Otherwise the result is over segmented.

$$r_{err} = \frac{n_{diff}}{N} \times 100\% \tag{18}$$

Low MAPE and r_{err} show low error, i.e high similarity with respect to the expert judgment. The testing dataset consist of 3 abscess, 4 haemorrhage, 11 acute infarction, and 2 tumour cases. In total, 23 samples are used for evaluation.

VIII. RESULTS

A. Thresholding Technique

Table 2 shows intensity of lesions on histogram thresholding. The threshold values are compared between Gamma-law transformation and contrast stretching. Minimum 0.48 and 0.28 are the optimal threshold value for the Gamma-law transformation and contrast stretching respectively.

Table 2 Optimal thresholding value

Optimal Threshold of Hyperintense Lesion			
Gamma-law Transformation		**Contrast Stretching**	
Min	Max	Min	Max
0.48	0.8	0.28	1.0

Fig. 14 shows segmentation results tested on our dataset as discussed in section III. The lesions are indicated by white circle. The first row of the images (i) represents the brain lesion images whereas the second row (ii) and the third row (iii) are the segmentation results using the

enhanced images after Gamma-law transformation and contrast stretching respectively. Both image enhancement techniques can successfully segment the lesions using thresholding.

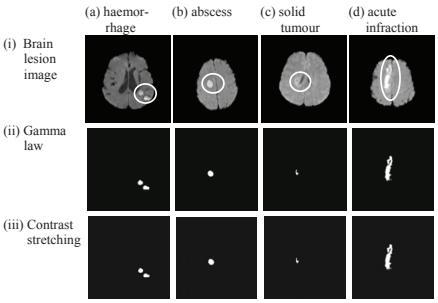

Fig. 14 Brain lesions and their segmentation results

Table 3 shows the performance evaluation between thresholding with Gamma-law transformation and contrast stretching algorithm.

Table 3 Performance evaluation for each lesion: Comparison between Gamma-law transformation and contrast stretching algorithm

Index	Area Overlap		False Positive Rate (over-segmentation)		False Negative Rate (under-segmentation)	
Tech-nique	Gamma -law	Contrast Stretch	Gamma-law	Contrast Stretch	Gamma-law	Contrast Stretch
Abscess	0.7042	0.6842	0.0296	0.0435	0.2662	0.2723
Haemor -rhage	0.6926	0.6763	0.1436	0.0909	0.1638	0.2328
Infarc-tion	0.7016	0.6492	0.1792	0.2213	0.1192	0.1404
Tumour	0.4893	0.2645	0.0923	0.0140	0.4183	0.7214
Average	0.6789	0.6214	0.1410	0.1478	0.1801	0.2308

The results show the segmentation of abscess, haemorrhage and infarction provide very good segmentation results. Thresholding with both algorithms provide high AO with low FPR and low FNR. These lesions were successfully segment by using our proposed thresholding technique because the lesions are very bright in DWI. From the table, the technique provides the worst result for all evaluation measurements for tumour. This is because, in DWI, the lesion for tumour is cannot fully characterized by its brightness. In addition, some tumour lesions in DWI comprise dark area in the middle or surrounding its hyperintense lesion which is failed to detect by histogram. Therefore, histogram thresholding provides low performance for tumour segmentation in DWI. The errors for under-segmentation (FNR) are bigger than over-segmentation (FPR) for all cases. The shaded areas show the best average performance. Fig. 15 shows average performance of lesion segmentation by using both Gamma-law transformation and contrast stretching algorithm.

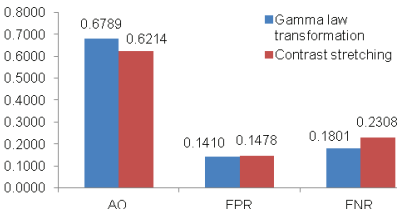

Fig. 15 Average performance of the thresholding algorithm

Gamma-law transformation algorithm provides higher AO which means better similarity to the manual segmentation provided by neuroradiologists. For over-segmentation (FPR) and under-segmentation (FNR) evaluation, gamma-law transformation provides higher performance, while contrast stretching gives poorer result. Overall, gamma-law transformation algorithm provides better segmentation results compared to contrast stretching.

B. GLCM

The proposed method has been tested with ten patients, as shown in Fig. 16. The images are normal; solid tumour, acute infarction, abscess and haemorrhage which represent hyperintense lesion; haemorrhage and chronic infarction which represent hypointense lesion.

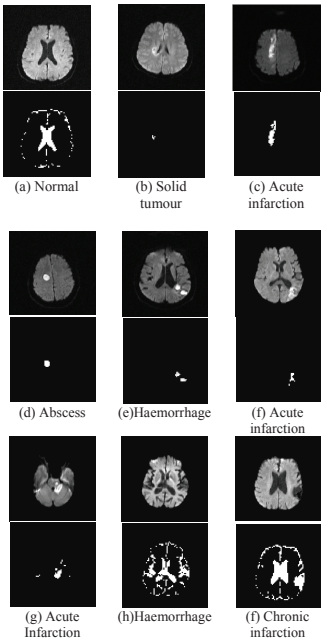

Fig. 16 Segmentation results. From top to bottom: (a) DWI for normal patient and segmentation result of normal CSF, (b-g) Segmentation of hyperintense lesions, (h-f) Segmentation of hypointense lesions

For normal patient in Fig. 16(a), the DWI is separated into two parts which are brain tissue and CSF in the middle of the brain. The results show that the normal brain tissue is well separated from the CSF. No hyperintense lesion is detected. Fig. 16 (b-g) shows several hyperintense lesions and their segmentation results. As seen in the figures, the lesions are well segmented using the approach method. Similar evaluation is made for the hypointense lesions in Fig. 16 (h-f). Since the hypointense lesions and CSF share similar characteristics, hence both regions fall under the hypointense regions. Normal CSF can be characterized by looking at the symmetrical shape in the middle of the brain while for hypointense lesion, the shape is irregular.

C. Segmentation Performance Comparison

Fig. 17 shows average performance of lesion segmentation by using both GLCM and thresholding. As discussed in the chapter VII, low MA, MAPE and rerr show low error, i.e high similarity with respect to the expert judgment. GLCM provides lower MA, MAPE and rerr compared to thresholding technique, which means more accurate. Overall, GLCM provides better segmentation results compared to thresholding technique.

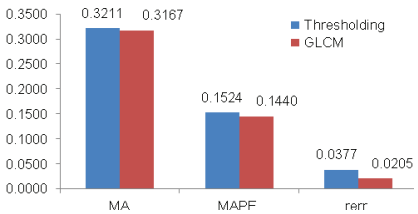

Fig. 17 Performance comparison between GLCM and thresholding

IX. CONCLUSIONS

This paper describes brain lesion segmentation in DWI using both thresholding technique and GLCM. Clinical DWI which focused on the hyperintense lesions which are infarction, acute haemorrhage, solid tumor and abscess are used for the study. Preprocessing stage is carried out for intensity normalization, background removal and intensity enhancement. Gamma-law transformation algorithm and contrast stretching are evaluated and compared to threshold the lesions. Images are segmented to 16 x 16 pixels size and histogram thresholding is applied at each region to find the maximum number of pixels. The result shows that both intensity enhancement techniques can be applied for successfully segment the hyperintense lesions using our proposed theresholding technique. However, Gamma-law transformation algorithm provides better segmentation results compared to contrast stretching. GLCM was also computed from the DWI. From the GLCM contour plot, GLCM cross section was constructed to compute the minimum and maximum threshold values. Region and boundary information from the GLCM were analyzed. The

GLCM regions that were according to hyperintense and hypointense lesions were segmented. The result shows that the proposed methods can successfully segment the lesions and is suitable for analysis of DWI and for classification purpose. Overall, GLCM provides better segmentation accuracy compared to thresholding technique.

ACKNOWLEDGMENT

The authors would like to thank Universiti Teknologi Malaysia (UTM) and Universiti Kebangsaan Malaysia Medical Centre (UKMMC) for collaboration in this research.

REFERENCES

[1] Malaysian Cancer Statistics – Data and Figure Peninsular Malaysia 2006, National Cancer Registry, Ministry of Health, Malaysia.

[2] American Cancer Society: Cancer Facts and Figures 2009. Atlanta, Ga: American Cancer Society, 2009.

[3] MAGNETOM Maestro Class: Diffusion Weighted MRI of the Brain. From brochure Siemens Medical Solutions that help.

[4] M. Ibrahim, N. John, M. Kabuka, A. Younis, "Hidden Markov models-based 3D MRI brain segmentation", Elsevier Journal of Image and Vision Computing Vol.24, 2006, pp. 1065–1079.

[5] S. J. Holdsworth, R. Bammer, "Magnetic Resonance Imaging Techniques: fMRI, DWI, and PWI", Seminars in Neurology, 2008 Vol.28, No. 4.

[6] P. W. Schaefer, P. E. Grant, R. G. Gonzalez, "State of the Art: Diffusion-weighted MR imaging of the brain", Annual Meetings of the Radiological Society of North America (RSNA), 2000, pp.331–345.

[7] S. K. Mukherji, T. L. Chenevert, M. Castillo, "State of the Art: Diffusion-Weighted Magnetic Resonance Imaging", Journal of Neuro-Ophthalmology Vol.22, No.2, 2002, pp. 118-122.

[8] R. Cardenes, R. de Luis-Garcia, M. Bach-Cuadra, "A multidimensional segmentation evaluation for medical image data" J. Computer Methods and Programs in Medicine, vol.96, 2009, pp.108-124.

[9] M.M. Trivedi, C.A. Harlow, R.W. Conners, S. Goh, "Object detection based on gray level cooccurrence." Computer Vision, Graphics, and Image Processing, 2:199-219, 1984.

[10] M.S. Khalil, D. Muhammad, M.K. Khan, Q. Al-Nuzaili, "Fingerprint Verification using Fingerprint Texture." Proceedings of the IEEE 2nd International Conference on Machine Vision, pp. 27-31, 2009.

[11] M.M. Mokji, S.A.R. Abu Bakar, "Adaptive thresholding based on co-occurrence matrix edge information." Proceedings of the 1st Asia International Conference on Modelling and Simulation, 2007.

[12] J. Webster (ed.), "Image Texture." Wiley Encyclopedia of Electrical and Electronics Engineering, John Wiley & Sons, Inc., 1999.

[13] N. Agani, S.A.R. Abu Bakar, S.H. Sheikh Salleh, "Application of texture analysis in echocardiography images for myocardial infarction tissue." Jurnal Teknologi, pp.61-76, Jun 2007.

[14] D.M-Ghoneim, "Cooccurrence histogram for characterizing brain magnetic resonance images." IEEE International Symposium on Signal Processing and Information Technology, 2009.

[15] H. S. Zadeh, F.R. Rad, *et.al*., "Comparison of multiwavelet, wavelet, Haralick, and shape features for microcalcifcation classification in mammograms." Elsevier Journals of Pattern Recognition, Vol.37, pp. 1973 – 1986, 2004.

[16] Norliza M.N., Omar M.R., Ashari Y., S.A.R. Abu-Bakar, "A discrimination method for the detection of pneumonia using chest radiograph."Computerized Medical Imaging and Graphics, vol.34, pp. 160-166, pp.160-166, 2010.

[17] Haralick, R.M., Shanmugam, K., Dinstein, I., "Texture parameters for image classification." IEEE Trans Systems, Man, Cybernetics, 3: 610-621, 1973.

[18] M. Barnathan, J. Zhang, E. Miranda, *et.al.*, "A Texture-Based Methodology for Identifying Tissue Type in Magnetic Resonance Images." IEEE International Symposium on Biomedical Imaging (ISBI): From Nano to Macro, pp.464-467, 2008.

[19] M. Torabi, R.D. Ardekani, E. Fatemizadeh, "Discrimination between Alzheimer's Disease and Control Group in MR-Images Based on Texture Analysis Using Artificial Neural Network." IEEE International Conference on Biomedical and Pharmaceutical Engineering, 2006.

[20] L.Wang, L. Tong, X. Liu, X. Li, C. Yu, "Study on normal appearing white matter of multiple sclerosis by texture analysis and modelling with MRI." IEEE International Conference on Information Acquisition, 2005.

[21] M. Ghazel, A. Traboulsee, R.K. Ward, "Semi-Automated Segmentation of Multiple Sclerosis Lesions in Brain MRI using Texture Analysis." IEEE International Symposium on Signal Processing and Information Technology, pp.6-10, 2006.

[22] J. Zhang, L. Wang, L. Tong, "Feature reduction and texture classification in MRI texture analysis of multiple sclerosis." IEEE/ICME International Conference on Complex Medical Engineering, pp. 752-757, 2007.

[23] W. Lin, X. Zhou, G. Jing, "Texture Analysis of MRI in Patients with Multiple Sclerosis Based on the Gray-level Difference Statistics." 1st International Workshop on Education Technology and Computer Science, pp.771-774, 2009.

[24] C. Chevrefils, F. Cheriet, C´ Eric Aubin, G. Grimard, "Texture Analysis for Automatic Segmentation of Intervertebral Disks of Scoliotic Spines from MR Images." IEEE Transaction on Information Technology and Biomedicine, vol. 13, No. 4, pp. 608-620, 2009.

[25] S. Cha "Review Article: Update on Brain Tumor Imaging: From Anatomy to Physiology", Journal of Neuroradiology, vol.27, pp.475-487, 2006.

[26] M.D.Hammer, L.R.Wechsler, "Neuroimaging in ischemia and infarction." Seminars in Neurology Vol.28, No. 4, 2008.

[27] R.T.Ullrich, L.W.Kracht, A.H.Jacobs "Neuroimaging in patients with gliomas." Seminars in Neurology, Vol.28, No. 4, 2008.

[28] O. Kastrup, I. Wanke, M. Maschke (2008) Neuroimaging of infections of the central nervous system, Seminars in Neurology, Vol.28, No. 4, 2008.

[29] J.F. Haddon, J.F. Boyce, "Co-occurrence matrices for image analysis." Electronics and Telecommunications Engineering Journal, pp.71-83, 1993.

[30] N. Mohd Saad, S. A. R. Abu-Bakar, Sobri Muda, Musa Mokji, "Automated Segmentation of Brain Lesion based on Diffusion-Weighted MRI using a Split and Merge Approach", Proceedings of 2010 IEEE-EMBS Conference on Biomedical Engineering & Sciences, IECBES 2010, 30th – 2nd Dec. 2010, Kuala Lumpur, Malaysia.

[31] R.C. Gonzalez, R.E. Woods, Digital Image Processing second edition, Prentice Hall, 2001.

[32] N. Mohd Saad, S. A. R. Abu-Bakar, Sobri Muda, M. M. Mokji, A. R. Abdullah, S. A. Mohd Chaculli, "Detection of Brain Lesions in Diffusion-weighted Magnetic Resonance Images using Gray Level Co-occurrence Matrix", Proceedings of the World Engineering Congress 2010 (WEC 2010), Kuching, Sarawak, Malaysia, pp.611-618.

[33] Rosniza Roslan, Nursuriati Jamil, Rozi Mahmud, "Skull Stripping of MRI Brain Images using Mathematical Morphology", Proceedings of 2010 IEEE-EMBS Conference on Biomedical Engineering & Sciences (IECBES 2010), 30th – 2nd Dec. 2010, Kuala Lumpur, Malaysia.